Optimizing flip angles for metabolic rate estimation in hyperpolarized carbon-13 MRI

John Maidens, *Student Member, IEEE,* Jeremy W. Gordon, Murat Arcak, *Fellow, IEEE,* and Peder E. Z. Larson, *Member, IEEE*

***Abstract*—Hyperpolarized carbon-13 magnetic resonance imaging has enabled the real-time observation of perfusion and metabolism *in vivo*. These experiments typically aim to distinguish between healthy and diseased tissues based on the rate at which they metabolize an injected substrate. However, existing approaches to optimizing flip angle sequences for these experiments have focused on indirect metrics of the reliability of metabolic rate estimates, such as signal variation and signal-to-noise ratio. In this paper we present an optimization procedure that focuses on maximizing the Fisher information about the metabolic rate. We demonstrate through numerical simulation experiments that flip angles optimized based on the Fisher information lead to lower variance in metabolic rate estimates than previous flip angle sequences. We then validate this optimized sequence *in vivo* with experiments in a prostate cancer mouse model. Based on these experiments we argue that our optimized sequence not only provides more reliable estimates of the metabolic rate, but also provides better estimates of other unknown parameters.**

***Index Terms*—Hyperpolarized carbon-13 magnetic resonance imaging, optimal experiment design, Fisher information, quantitative imaging, parameter mapping**

I. Introduction

HYPERPOLARIZED carbon-13 magnetic resonance imaging (MRI) has enabled the real-time observation of perfusion and metabolism in preclinical and clinical studies [1]–[6]. This technology is made possible by techniques for dynamic nuclear polarization (DNP) that have led to signal-to-noise ratio (SNR) increases of four to five orders of magnitude compared with endogenous signal in dissolved ^{13}C-labelled molecules [7], [8]. Injected [1-^{13}C] pyruvate is frequently used as a substrate in metabolism experiments and its rate of conversion to [1-^{13}C] lactate has been shown to distinguish between healthy and diseased tissues in animal [2], and recently human [4], studies.

In contrast with conventional MRI, magnetization is a non-renewable resource in hyperpolarized MRI. Conventional imaging relies only on thermal equilibrium polarization, therefore an arbitrary number of acquisitions can be performed if we allow time for the magnetization to return to equilibrium between acquisitions. In contrast, hyperpolarization can only be performed before a ^{13}C-labeled substrate is injected into the body, and once injected the magnetization decays due to T_1 relaxation and rapid T_2 relaxation following radio frequency (RF) excitation. Thus, the choice of excitation sequence is important for managing the trade-off between present and future measurement quality.

In typical practice a constant flip angle sequence is used for excitation, with typical values ranging from 5–30 degrees. Alternative time-varying acquisition sequences include sequences that attempt to maintain constant observed signal over time [9], maximize the cumulative observed lactate signal over time [10], or saturate the lactate signal in each acquisition [11].

In this paper our goal is to design a time-varying flip angle sequence to achieve maximally reliable quantitative estimates of the metabolic rate that can be compared between tissue regions, across subjects, or over time. We achieve this goal by developing a statistical model of the observed data as a function of the flip angle sequence and designing flip angles to maximize the Fisher information about the metabolic rate parameter.

We begin by presenting a mathematical model of the magnetization dynamics in the observed tissue in Section II. In Section III, we introduce a flip angle optimization procedure and present an optimal sequence. Next, we validate this result with computer simulation studies to demonstrate that our optimized sequence yields more reliable metabolic rate estimates than commonly-used constant and RF compensated flip angle sequences in Section IV. Finally, in Section V, we demonstrate the feasibility of this procedure *in vivo* and validate our mathematical model with a sequence of experiments in a prostate cancer mouse model.

The software and experimental data required to generate the figures in this paper are available at: https://github.com/maidens/TMI-2015.

II. Mathematical Model

We consider a two-dimensional system of ordinary differential equations

$$\frac{dx}{dt}(t) = \begin{bmatrix} -k_{PL} - R_{1P} & 0 \\ k_{PL} & -R_{1L} \end{bmatrix} x(t) + \begin{bmatrix} k_{TRANS} \\ 0 \end{bmatrix} u(t) \quad (1)$$

that models the magnetization dynamics in a tissue with an arterial input function $u(t)$ and uni-directional conversion from the substrate (pyruvate) to a metabolic product (lactate), which has been commonly applied for hyperpolarized ^{13}C pyruvate experiments. The state $x_1(t)$ denotes the longitudinal magnetization of pyruvate contained in a particular voxel in

J. Maidens and M. Arcak are with the Department of Electrical Engineering & Computer Sciences, University of California, Berkeley, CA, 94720, USA. e-mail: {maidens, arcak}@eecs.berkeley.edu

J. Gordon and P. Larson are with the Department of Radiology and Biomedical Imaging, University of California, San Francisco, 1700 4th Street, San Francisco, CA, 94158, USA. e-mail: {jeremy.gordon, peder.larson}@ucsf.edu

Research supported in part by NSERC postgraduate fellowship PGFD3-427610-2012 and NIH grants R00-EB012064, R01-EB016741 and P41-EB013598.

the tissue and $x_2(t)$ the longitudinal magnetization of lactate in the same voxel. The rate of metabolism of pyruvate to lactate is denoted k_{PL}, the perfusion rate from the arterial input to the tissue is denoted k_{TRANS}, and R_{1P} and R_{1L} are lumped parameters that account for T_1 decay in the magnetization along with other effects, such as metabolism of pyruvate into products other than lactate as well as flow of magnetization out of the slice. The input to the system $u(t)$ is an unmeasured arterial input function (AIF) resulting from the injection of hyperpolarized [1-^{13}C] pyruvate. In an experimental setting an AIF will be estimated based on the data collected, but for the purposes of designing a flip angle sequence, it will be assumed to be of gamma-variate shape

$$u(t) = A_0(t - t_0)^{\gamma} e^{-(t-t_0)/\beta}$$

with parameters t_0, γ, β, A_0 given in Table I.

We acquire data at N time points separated by intervals of length T_R. Each time t an acquisition is made, we must choose a flip angle $\alpha_{k,t}$ for each compound k to be measured. If the magnetization of the k-th compound before the acquisition is x_k, then this choice of flip angle allows us to measure a signal of magnitude $\sin(\alpha_{k,t})x_k$, after which $\cos(\alpha_{k,t})x_k$ magnetization remains for future acquisitions (Fig. 1a). This causes discrete jumps, or resets, in the system state, leading to a hybrid dynamical system [12], [13] (Fig. 1b). Since we are only interested in the system's state at acquisition times, we can avoid technicalities associated with hybrid system modelling by discretizing the system in time and considering a discrete-time dynamical system that simultaneously captures the evolution of (1) between acquisitions and the discrete jumps induced by the acquisitions. We define the transition matrices A_d and B_d

$$A_d = \exp\left(T_R \begin{bmatrix} -k_{PL} - R_{1P} & 0 \\ k_{PL} & -R_{1L} \end{bmatrix}\right)$$

$$B_d = \begin{bmatrix} -k_{PL} - R_{1P} & 0 \\ k_{PL} & -R_{1L} \end{bmatrix}^{-1} (A_d - I) \begin{bmatrix} k_{TRANS} \\ 0 \end{bmatrix}$$

that correspond to the discretization of (1) assuming a zero-order hold on the input between each acquisition [14].

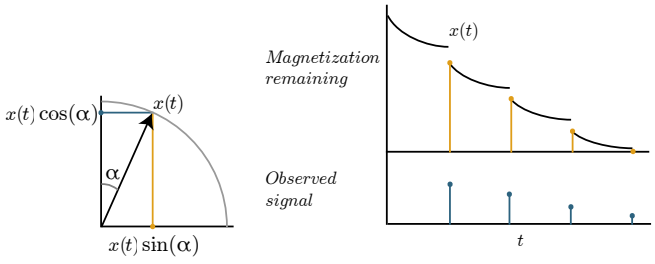

(a) Flip angle selection (b) Hybrid (continuous-discrete) dynamics

Fig. 1. Illustration of the trade-off between present and future image intensity in a single compound. (a) Each acquisition relies on choosing an angle α to perturb the longitudinal magnetization into the transverse plane, allowing a measurement of magnitude $x(t)\sin(\alpha)$, after which $x(t)\cos(\alpha)$ longitudinal magnetization remains for future acquisitions. (b) Repeated excitation leads to repeated discrete jumps in the system state, depleting the remaining magnetization.

The measurements acquired are modelled as independent Rician-distributed random variables [15], which have probability density

$$p_{x,\sigma}(y) = \frac{y}{\sigma^2} \exp\left(-\frac{y^2 + x^2}{2\sigma^2}\right) I_0\left(\frac{yx}{\sigma^2}\right)$$

where I_ν denotes the modified Bessel function of the first kind of order ν. All together, we have the discrete-time model

$$\begin{aligned} x_0 &= 0 \\ x_{t+1} &= A_d(\theta) \begin{bmatrix} \cos\alpha_{1,t} & 0 \\ 0 & \cos\alpha_{2,t} \end{bmatrix} x_t + B_d(\theta) u_t(\theta) \\ \tilde{x}_{k,t} &= \sin(\alpha_{k,t}) x_{k,t} \quad k = 1, 2 \\ Y_{k,t} &\sim Rice(\tilde{x}_{k,t}, \sigma_k) \quad k = 1, 2. \end{aligned} \tag{2}$$

Simulated trajectories of this model are shown in Fig. 2.

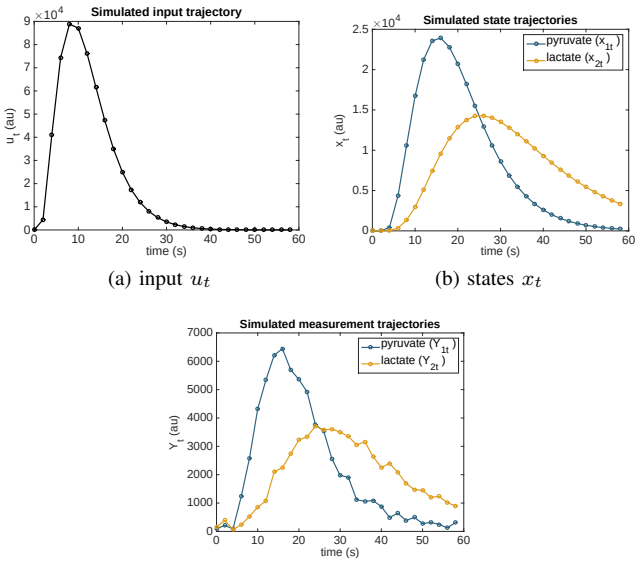

(a) input u_t (b) states x_t

(c) Rician-distributed measurements Y_t

Fig. 2. Simulated trajectories of the model (2) using a constant flip angle sequence with $\alpha_{k,t} = 15°$.

The model parameters are

$$\theta = [R_{1P}, R_{1L}, k_{PL}, k_{TRANS}, u_0, \ldots, u_{N-1}]$$

and we have the freedom to choose

$$\alpha = \begin{bmatrix} \alpha_{1,1} & \ldots & \alpha_{1,N} \\ \alpha_{2,1} & \ldots & \alpha_{2,N} \end{bmatrix}$$

to generate the best possible estimate of the unknown parameters. The noise parameters σ_k for $k = 1, 2$ can be estimated separately from a measurement of the background and are therefore assumed to be known. We fix a sampling interval of $T_R = 2$ seconds, though this could in principle be included as a decision variable.

III. Optimal Experiment Design

In this section, we present a sequence of flip angles that provides maximal information about the metabolic rate parameter k_{PL}. This optimization problem is solved in MATLAB using

a toolbox we have developed for the design of optimal flip angle sequences. This toolbox is open source and available at https://github.com/maidens/Flip-Angle-Design-Toolbox.

A. Fisher information

The optimal design of experiments allows the estimation of model parameters from observed data with minimum variance in the estimates [16]. The Cramér-Rao bound

$$\mathrm{cov}(\hat{\theta}) \geq \mathcal{I}^{-1}$$

gives a lower bound on the covariance of any unbiased estimator $\hat{\theta}$ of the parameter θ in terms of the Fisher information matrix, the positive semidefinite matrix with entries

$$\mathcal{I}_{ij} = \mathbb{E}\left[\frac{\partial \log p_\theta(y)}{\partial \theta_i}\frac{\partial \log p_\theta(y)}{\partial \theta_j}\middle| \theta, \alpha\right].$$

Under mild assumptions, the maximum likelihood estimator is asymptotically efficient [17], that is, it achieves the Cramér-Rao bound as the amount of data collected tends to infinity. Thus, to find a maximum-likelihood estimate with minimum variance, we choose the sequence α to maximize the Fisher information matrix at a nominal value of the parameter vector θ. The nominal parameter values used are given in Table I and were chosen based on our typical data in a prostate cancer mouse model.

R_{1P}	R_{1L}	k_{PL}	k_{TRANS}	t_0	γ	β	A_0	σ_k
1/20	1/20	0.07	0.055	3.2596	2.1430	3.4658	1.0411 $\times 10^4$	2.3608 $\times 10^4$

TABLE I
NOMINAL PARAMETER VALUES USED TO COMPUTE OPTIMAL FLIP ANGLE SEQUENCES

To compute the Fisher information, we use the expression derived in [18] for the (i,j)-th entry of $\mathcal{I}$:

$$\mathcal{I}_{ij} = \sum_{t=0}^{N}\sum_{k=1}^{2}\frac{1}{\sigma_k^2}\frac{\partial \tilde{x}_{k,t}}{\partial \theta_i}\frac{\partial \tilde{x}_{k,t}}{\partial \theta_j}\psi\left(\frac{\tilde{x}_{k,t}}{\sigma_k}\right) \tag{3}$$

where the sensitivities are computed recursively as

$$\begin{cases} \frac{\partial x_0}{\partial \theta_i} = 0 \\ \frac{\partial x_{t+1}}{\partial \theta_i} = \frac{\partial A_d}{\partial \theta_i}\begin{bmatrix}\cos\alpha_{1,t} & 0\\ 0 & \cos\alpha_{2,t}\end{bmatrix}x_t \\ \qquad\qquad + A_d\begin{bmatrix}\cos\alpha_{1,t} & 0\\ 0 & \cos\alpha_{2,t}\end{bmatrix}\frac{\partial x_t}{\partial \theta_i} + \frac{\partial B_d}{\partial \theta_i}u_t + B_d\frac{\partial u_t}{\partial \theta_i} \\ \frac{\partial \tilde{x}_t}{\partial \theta_i} = \begin{bmatrix}\sin\alpha_{1,t} & 0\\ 0 & \sin\alpha_{2,t}\end{bmatrix}\frac{\partial x_t}{\partial \theta_i} \end{cases}$$

and ψ is defined in terms of the integral

$$\psi(z) = -z^2 + \int_0^\infty y^3 \frac{I_1^2(yz)}{I_0(yz)}\exp\left(-\frac{1}{2}(y^2+z^2)\right)dy.$$

B. Eliminating nuisance parameters

In practice, we do not necessarily need good estimates of all the unknown parameters in the model. For example, in this paper our primary goal is to estimate the metabolic rate parameter k_{PL} which is useful for discriminating between cancerous and non-cancerous tissues [5], determining the severity of disease [19], [20] and monitoring response to therapy [2]. Thus we wish to modify our optimality criterion to maximize the sensitivity of the experiments to k_{PL} while considering the nuisance parameters only insofar as they allow us to estimate the parameters of interest. We do so by partitioning the information matrix as

$$\mathcal{I} = \begin{bmatrix}\mathcal{I}_{11} & \mathcal{I}_{12}\\ \mathcal{I}_{21} & \mathcal{I}_{22}\end{bmatrix}$$

where the first block corresponds to the parameters of interest and the second block corresponds to the nuisance parameters. Optimal design for the parameters of interest can then be performed by maximizing the Schur complement of $\mathcal{I}_{22}$:

$$\mathcal{S} = \mathcal{I}_{11} - \mathcal{I}_{12}\mathcal{I}_{22}^{-1}\mathcal{I}_{21}$$

which corresponds to minimizing the asymptotic covariance of the marginal distribution corresponding to the parameters of interest (see Section 6.1 of [21]).

In general, if multiple parameters are of interest then $\mathcal{S}$ will be a matrix and we would be required to choose a suitable scalar criterion for measuring the size of $\mathcal{S}$. The problem of simultaneously estimating k_{PL} and k_{TRANS} is considered in [18], where the $D-$, $E-$ and $A-$ optimality criteria are compared. However, in this instance we are considering a single parameter of interest k_{PL}, therefore the Schur complement $\mathcal{S}$ is scalar-valued.

C. Regularization

We desire a smoothly-varying sequence of flip angles for a number of reasons including increasing robustness against model mismatch and interpretability of the resulting sequence of flip angles. We achieve smoothness in the flip angle sequence by adding a regularization term $\lambda\|\Delta\alpha\|_F$ to the objective function to penalize nonsmooth sequences where the differencing operator Δ is defined as

$$\Delta\left(\begin{bmatrix}\alpha_{1,1} & \dots & \alpha_{1,N}\\ \alpha_{2,1} & \dots & \alpha_{2,N}\end{bmatrix}\right) = \begin{bmatrix}(\alpha_{1,2}-\alpha_{1,1}) & \dots & (\alpha_{1,N}-\alpha_{1,N-1})\\ (\alpha_{2,2}-\alpha_{2,1}) & \dots & (\alpha_{2,N}-\alpha_{2,N-1})\end{bmatrix}$$

and $\|\cdot\|_F$ denotes the Frobenius norm. The nonnegative parameter λ can be adjusted to achieve the desired degree of smoothness. The flip angle sequence shown here is computed using the value $\lambda = 0.1$.

D. Numerical optimization

To design an optimal flip angle scheme, we must solve the flip angle optimization problem

$$\underset{\alpha}{\text{maximize}}\ \mathcal{S}(\theta,\alpha) - \lambda\|\Delta\alpha\|_F \tag{4}$$

for the flip angle sequence α where θ is fixed to some nominal value for the unknown parameters. The MATLAB Optimization Toolbox [22] provides a derivative-free implementation of the quasi-Newton optimization algorithm of Broyden-Fletcher-Goldfarb-Shanno (BFGS) [23], which is well-suited to finding local optima of this objective function.

E. Results

A solution to the optimization problem (4), initialized at $\alpha_{k,t} = 5°$, is given in Fig. 3. Simulated state and observation trajectories corresponding to this flip angle sequence are shown in Fig. 4.

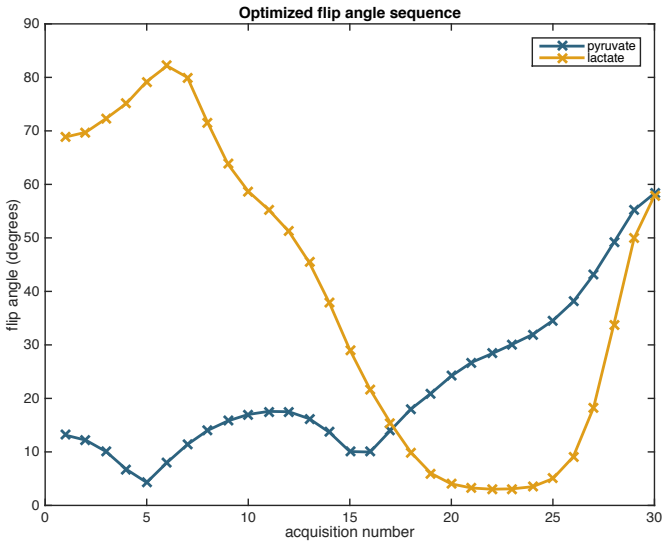

Fig. 3. Optimized flip angle sequence for estimating the metabolic rate parameter k_{PL} using the nominal parameter values in Table I and a sampling interval T_R = 2 s between acquisitions.

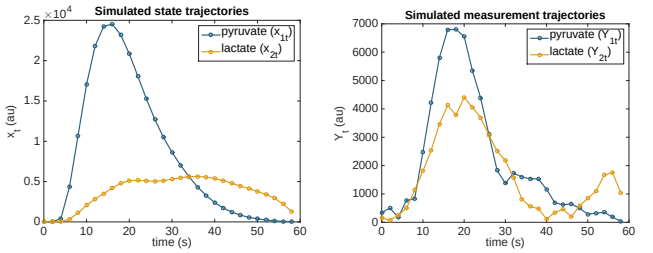

(a) states x_t (b) Rician-distributed measurements Y_t

Fig. 4. Simulated trajectories of the model (2) using the optimized flip angle sequence shown in Fig. 3 and the arterial input function shown in Fig. 2a.

We see that the pyruvate flip angles follow a pattern similar to flip angle sequences designed for other objectives, beginning with small flip angles to preserve magnetization for future acquisitions but increasing toward the end of the sequence [9], [10]. In contrast, the optimized flip angle sequence is much more aggressive with the lactate flip angles at the beginning of the experiment than in other variable flip angle sequences. This provides more reliable information about the leading end of the lactate time series, which contains the most information about the metabolic rate.

IV. Validation Using Simulated Data

In this section, we demonstrate the advantage of the optimally designed flip angle sequence using computer-simulated data. Working with simulated data allows us to collect a large number of statistically independent data sets and provides us access to a "ground truth" value for the parameter vector. This makes it possible to reliably determine the parameter estimation error that results from noise in the simulated measurements. It is not feasible to acquire such a large number of data sets *in vivo*, and these would also not include ground truth values. Thus we use simulated data to demonstrate that our optimized flip angle sequence leads to smaller uncertainty in estimates of the metabolic rate parameter k_{PL}.

A. Two-step parameter estimation procedure

When fitting the data from *in vivo* experiments, data from different voxels will correspond to different values of the parameters k_{TRANS}, k_{PL}, R_{1P} and R_{1L} as these values change with spatial location, but all correspond to the same arterial input $u(t)$. Thus we present a fitting procedure that proceeds in two steps: first we fit a single input function $u(t)$ to the entire data set, then we fix this input function and estimate values of the remaining parameters individually for each of the voxels in the slice.

B. Results

We wish to compare the reliability of estimates of k_{PL} between data generated using: 1) the optimized flip angle sequence (given in Fig. 3), 2) a constant flip angle sequence of 15°, and 3) an RF compensated flip angle sequence that aims to keep the measured signal constant despite repeated RF excitation (Fig. 9b). For each of the three flip angle sequences, we simulate $n = 25$ independent data sets from the model (2) using the parameter values given in Table I. We then perform the two-step parameter estimation procedure described in Section IV-A. The resulting parameter estimates are shown in Fig. 5. We see that for all three flip angle sequences, the parameter estimates congregate near the ground truth value of the model parameters.

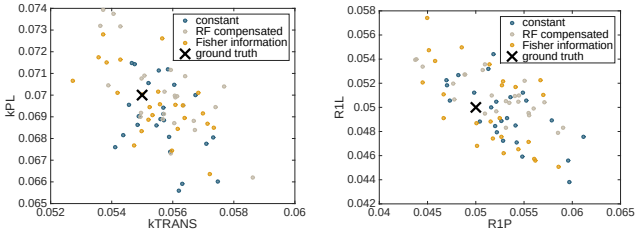

(a) k_{TRANS} and k_{PL} (b) R_{1P} and R_{1L}

Fig. 5. Maximum likelihood estimates of the parameters k_{TRANS}, k_{PL}, R_{1P} and R_{1L} for numerous independent simulated data sets compared between three flip angle sequences for $\sigma^2 = 2.3608 \times 10^4$. The ground truth value is depicted as $\times$.

To demonstrate that our optimized flip angle sequence provides more accurate estimates of k_{PL} than the competing flip angle sequences, we compare the root mean squared (RMS) estimation error between the sequences. We repeat this experiment for various values of the noise parameter σ^2 ranging from 10^3 to 10^6 to demonstrate that the improvement in the estimates is robust to variation in the noise strength. A value of approximately 2×10^4, in the center of this range,

is typical for prostate tumor mouse model experiments. For each value of σ^2 we compute the RMS error of the k_{PL} and nuisance parameter estimates across the $n = 25$ trajectories and plot these relationships in Figs. 6 and 7 respectively. We see that the optimized flip angle sequence provides a more reliable estimate of the parameter of interest k_{PL}, though at the expense of less reliable estimates of the nuisance parameter R_{1L}.

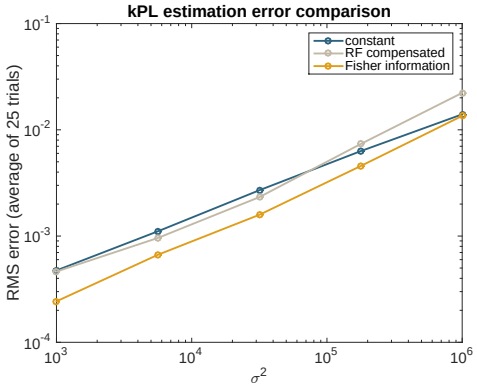

Fig. 6. Comparison of the root mean square k_{PL} estimation error between various flip angle sequences across different values of the noise strength parameter σ^2.

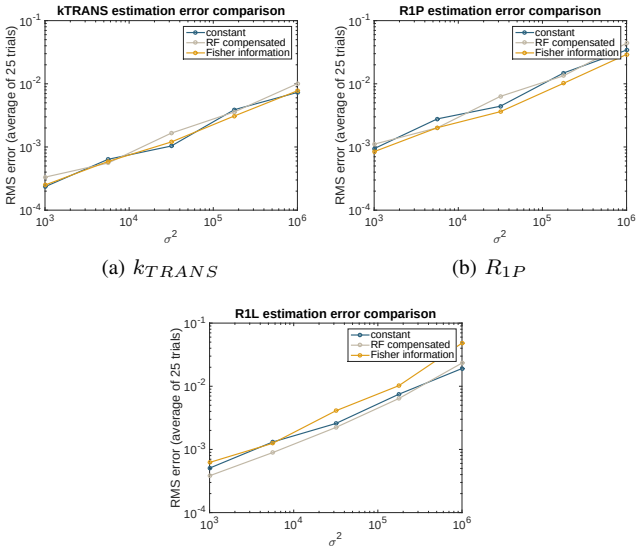

(a) k_{TRANS} (b) R_{1P}

(c) R_{1L}

Fig. 7. Comparison of the root mean square nuisance parameter estimation error between various flip angle sequences across different values of the noise strength parameter σ^2.

V. In Vivo Results

We now move on to *in vivo* experiments. In contrast with the *in silico* experiments, here there is no ground truth value of the model parameters against which to compare our estimates, as the true rates are unknown and may vary between different regions of the tissue. However, the *in vivo* experiments can be used to validate the model that we have chosen and to demonstrate the feasibility of model-based parameter mapping using our optimized time-varying flip angle sequence. We show that our model can reliably reproduce observed data and achieve consistent parameter estimates across a variety of time-varying flip angle sequences.

A. Experimental setup

To validate this technique *in vivo*, metabolic data were acquired in a prostate tumor mouse (TRAMP) model using a 3T MRI scanner (MR750, GE Healthcare). Briefly, 24μL aliquots of [1-^{13}C] pyruvic acid doped with 15mM Trityl radical (Ox063, GE Healthcare) and 1.5mM Dotarem (Guerbet, France) were inserted into a Hypersense polarizer (Oxford Instruments, Abingdon, England) and polarized for 60 minutes. The sample was then rapidly dissoluted with 4.5g of 80mM NaOH/40mM Tris buffer to rapidly thaw and neutralize the sample. Following dissolution, 450μL of 80mM pyruvate was injected via the tail vein over 15 seconds, and data acquisition coincided with the start of injection. Metabolites from a single slice were individually excited with a singleband spectral-spatial RF pulse and encoded with a single-shot symmetric EPI readout [24], with a repetition time of 100ms, a field-of-view of 53 $\times$ 53mm, a matrix size of 16 $\times$ 16, an 8mm slice thickness, and a 2 second sampling interval. A ^{1}H image showing the anatomy contained in the slice in question is given in Fig. 8.

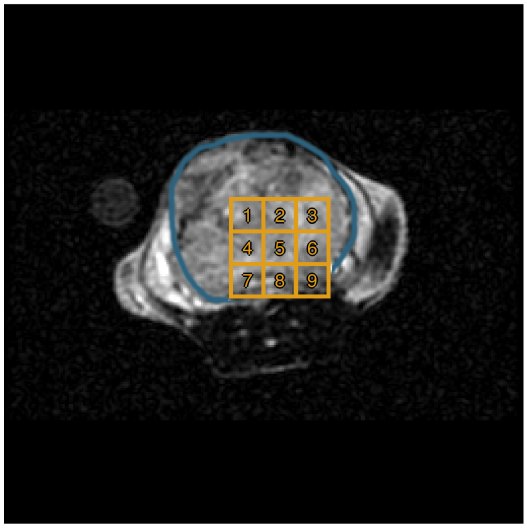

Fig. 8. ^{1}H image of the slice of interest. A large tumor, outlined in blue, fills a significant portion of the slice. Numbered volumes used to extract trajectories for parameter estimation in Section V-D are outlined in gold.

Datasets were acquired using three time-varying flip angle sequences. The T_1-effective and RF-compensated sequences, shown in Figs. 9a and 9b respectively, aim to distribute observed magnetization evenly across acquisitions, leading to roughly constant observed signals over time. The RF-compensated sequence does so by accounting for magnetization lost due to repeated RF excitation, but ignoring exchange between chemical compounds and T_1 relaxation [25]. In contrast, the T_1-effective sequence accounts for exchange and T_1 relaxation as well as RF excitation in attempting to achieve

a flat time profile [9]. We compare these two sequences against our sequence, shown in Fig. 3, that has been optimized with respect to the Fisher information about k_{PL}.

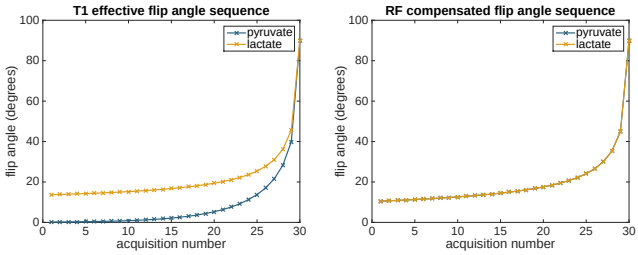

(a) T_1 effective (b) RF compensated

Fig. 9. Flip angle schedules compared experimentally with our optimized flip angle sequence. Note that for the RF compensated schedule, the sequences corresponding to pyruvate and lactate are identical.

B. Resulting data

An example of the collected data, from the experiment with the Fisher information-optimized flip angles, is shown in Fig. 10.

C. Flip angle profile modelling

Due to an imperfect (non-rectangular) slice profile, flip angles applied in practice vary spatially across the slice. This can lead to excess signal coming from regions near the boundary of the slice at later time points in the acquisitions, a phenomenon known as the slice profile effect [26], [27]. We have found that it is necessary to account for this effect in order to accurately fit the experimental data.

We consider the actual slice profile $\pi(z)$ shown in Fig. 11 which corresponds to the spatial response of the RF pulse used experimentally. We assume that at each time step t and for each compound k (*i.e.* $k = 1$ corresponding to pyruvate, $k = 2$ corresponding to lactate) we can choose a real parameter $\alpha_{k,t}$ such that the flip angle applied at location z is $\theta_{k,t}(z) = \alpha_{k,t}\pi(z)$. To generate a finite-dimensional model of the dynamics, we consider the magnetization dynamics at a discrete set of z coordinates $\{z_1, \ldots, z_N\}$. The magnetization at location z_i in the slice is then governed by the equations

$$x_{i,t+1} = A_d \begin{bmatrix} \cos(\alpha_{1,t}\pi(z_i)) & 0 \\ 0 & \cos(\alpha_{2,t}\pi(z_i)) \end{bmatrix} x_{i,t} + B_d u_t(p)$$

and the total magnetization measured is then assumed to be distributed

$$\tilde{x}_t = \sum_{i=1}^{N} \frac{1}{z_{i+1} - z_i} \begin{bmatrix} \sin(\alpha_{1,t}\pi(z_i)) & 0 \\ 0 & \sin(\alpha_{2,t}\pi(z_i)) \end{bmatrix} x_{i,t}$$

$$Y_{k,t} \sim Rice(\tilde{x}_{k,t}, \sigma^2).$$

This approach accounts for the slice profile effects by modelling the dynamics across the actual slice profile.

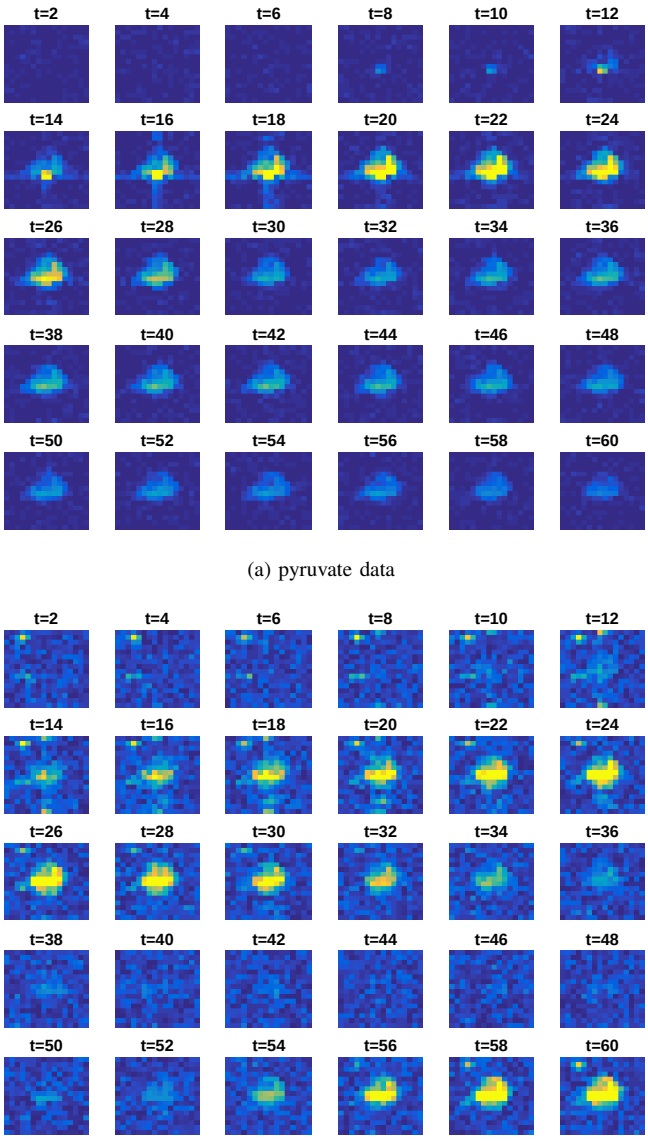

(a) pyruvate data

(b) lactate data

Fig. 10. Data collected using the optimized flip angles shown in Fig. 3. The field-of-view of these images is identical to the ^{1}H image in Fig. 8.

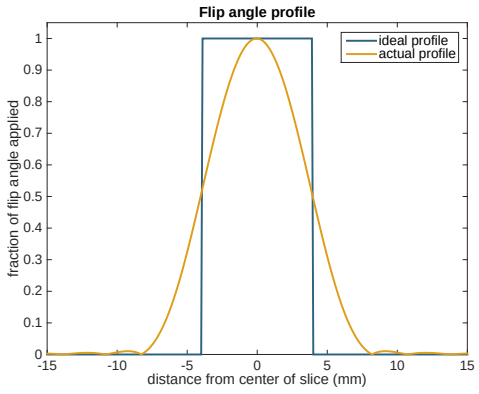

Fig. 11. Comparison between an ideal flip angle profile across the slice and the actual profile for the RF excitation pulse used.

D. Parameter estimation

We begin by extracting time evolutions of the measured pyruvate and lactate signal from $n = 9$ voxels in the slice. The chosen volumes from which these signals are extracted are illustrated in Fig. 8. As in Section IV, parameter estimation is performed in two steps. First, a single arterial input function and value for the parameter R_{1L} are estimated based on the spatial average of the time series extracted from the tumor region. Second, the estimated input function and R_{1L} value are held fixed while model parameters k_{TRANS} and k_{PL} are fit individually to the time series extracted from each of the voxels. To ensure practical identifiability of the model, the parameter R_{1P} is fixed to a value of 0.05 during both steps.

Estimates of the arterial input corresponding to each of the three flip angle sequences are shown in Fig. 12. We see that the estimated inputs are reasonably consistent between the three data sets, but have some variation due to measurement noise in the pyruvate signal. Our optimized sequence yields the most smoothly-varying input function, which suggests that it is likely the most reliable of the three estimated AIFs.

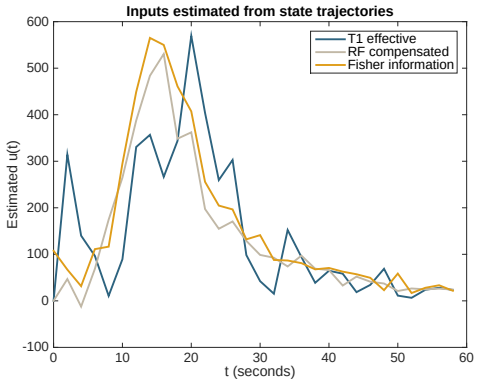

Fig. 12. Estimated arterial input functions corresponding to each of the three flip angle sequences given in Figs. 3 and 9.

Parameter estimates corresponding to each of the nine voxels are compared between the three flip angle sequences in Fig. 13. Examples of the quality of the fit corresponding to a particular voxel are shown in Fig. 14. We see that the estimated parameter values are consistent between the three flip angle sequences and that our model is able to reliably reproduce the observed data in all three cases. This provides evidence that the model we have used in this paper accurately describes the dynamics of magnetization exchange *in vivo*, and hence that the reliability results that we have demonstrated in the simulation experiments of Section IV are valid.

E. Parameter mapping

We now present maps that show the spatial distribution of estimated metabolic and perfusion rates in Fig. 15. We see that the range and spatial distribution of parameter estimates are similar between acquisition sequences, further validating our model.

VI. Conclusion

We have presented a method of generating optimal flip angle sequences for estimating the metabolic rate in a model of

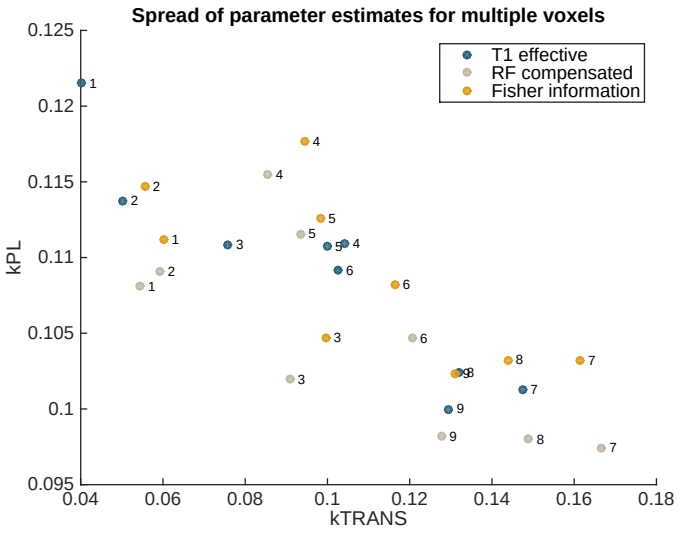

Fig. 13. Maximum likelihood estimates of the parameters k_{TRANS} and k_{PL} for time series trajectories extracted from various voxels, labelled 1 through 9. The resulting estimates are compared between data sets collected using the three flip angle sequences shown in Figs. 3 and 9.

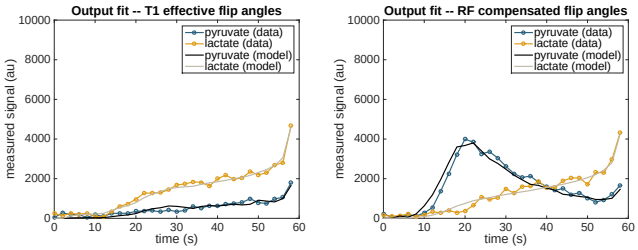

(a) T_1 effective flip angle sequence (Fig. 9a)

(b) RF compensated flip angle sequence (Fig. 9b)

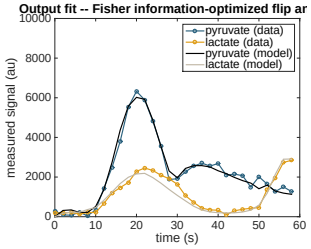

(c) Fisher information optimized flip angle sequence (Fig. 3)

Fig. 14. Model fit to a collection of experimentally measured time series data corresponding to voxel number 5. Each of the three data sets was collected using a different flip angle sequence.

pyruvate metabolism. This method uses the Fisher information about the parameter of interest as the objective function that we wish to maximize. We have shown that the resulting flip angle sequence leads to smaller variance in the parameter estimates due to noise in the measured signal. We have demonstrated this first *in silico* where we can explicitly compare the estimated model parameter values against the ground truth value. We also performed *in vivo* experiments to validate the model used in the *in silico* experiments and to demonstrate the feasibility of metabolic rate estimation and parameter mapping using this novel sequence. Overall our results provide evidence that,

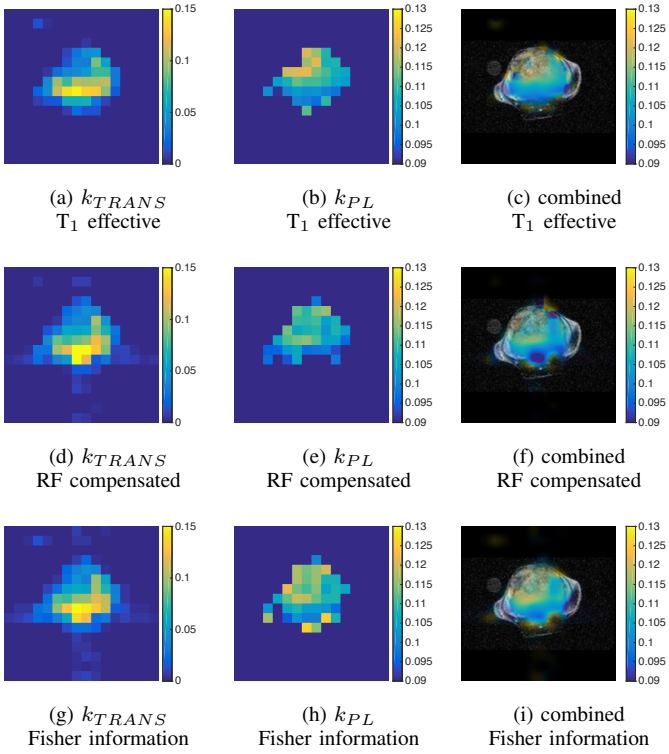

(a) k_{TRANS} T_1 effective (b) k_{PL} T_1 effective (c) combined T_1 effective

(d) k_{TRANS} RF compensated (e) k_{PL} RF compensated (f) combined RF compensated

(g) k_{TRANS} Fisher information (h) k_{PL} Fisher information (i) combined Fisher information

Fig. 15. Maps of the perfusion rate parameter k_{TRANS} and metabolic rate parameter k_{PL} corresponding to each of the three flip angle sequences. The k_{PL} maps are masked outside the perfused region using a threshold of $k_{TRANS} = 0.02$. A single map combining anatomic, perfusion and metabolism information is shown on the right. In this map, the color is determined by the estimated k_{PL} value while the transparency of the map is set using the perfusion rate parameter k_{TRANS} such that in highly-perfused tissues where the estimates of the metabolic rate parameter are more reliable the map is less transparent. The combined image data are zero-filled from 16 $\times$ 16 to 256 $\times$ 256 to match the resolution of the ^{1}H images.

for experiments that aim to quantitatively compare metabolic rates, optimizing flip angle sequences based on the Fisher information leads to more reliable estimates of the model parameters of interest.

REFERENCES

[1] K. Golman and S. J. Petersson, "Metabolic imaging and other applications of hyperpolarized ^{13}C^1," *Academic Radiology*, vol. 13, no. 8, pp. 932–942, Aug. 2006.

[2] S. E. Day, M. I. Kettunen, F. A. Gallagher, D.-E. Hu, M. Lerche, J. Wolber, K. Golman, J. H. Ardenkjær-Larsen, and K. M. Brindle, "Detecting tumor response to treatment using hyperpolarized ^{13}C magnetic resonance imaging and spectroscopy," *Nature Medicine*, no. 11, pp. 1382–1387, 2007.

[3] S. M. Kazan, S. Reynolds, A. Kennerley, E. Wholey, J. E. Bluff, J. Berwick, V. J. Cunningham, M. N. Paley, and G. M. Tozer, "Kinetic modeling of hyperpolarized ^{13}C pyruvate metabolism in tumors using a measured arterial input function," *Magnetic Resonance in Medicine*, vol. 70, no. 4, pp. 943–953, 2013.

[4] S. J. Nelson, J. Kurhanewicz, D. B. Vigneron, P. E. Z. Larson, A. L. Harzstark, M. Ferrone, M. van Criekinge, J. W. Chang, R. Bok, I. Park, G. Reed, L. Carvajal, E. J. Small, P. Munster, V. K. Weinberg, J. H. Ardenkjær-Larsen, A. P. Chen, R. E. Hurd, L.-I. Odegardstuen, F. J. Robb, J. Tropp, and J. A. Murray, "Metabolic imaging of patients with prostate cancer using hyperpolarized [1-^{13}C]pyruvate," *Science Translational Medicine*, vol. 5, no. 198, p. 198ra108, 2013.

[5] N. Bahrami, C. L. Swisher, C. von Morze, D. B. Vigneron, and P. E. Z. Larson, "Kinetic and perfusion modeling of hyperpolarized ^{13}C pyruvate and urea in cancer with arbitrary RF flip angles," *Quantitative Imaging in Medicine and Surgery*, vol. 4, no. 1, 2014.

[6] C. L. Swisher, P. E. Z. Larson, K. Kruttwig, A. B. Kerr, S. Hu, R. A. Bok, A. Goga, J. M. Pauly, S. J. Nelson, J. Kurhanewicz, and D. B. Vigneron, "Quantitative measurement of cancer metabolism using stimulated echo hyperpolarized carbon-13 MRS," *Magnetic Resonance in Medicine*, vol. 71, no. 1, pp. 1–11, 2014.

[7] J. H. Ardenkjær-Larsen, B. Fridlund, A. Gram, G. Hansson, L. Hansson, M. H. Lerche, R. Servin, M. Thaning, and K. Golman, "Increase in signal-to-noise ratio of $>$ 10,000 times in liquid-state NMR," *Proceedings of the National Academy of Sciences*, vol. 100, no. 18, pp. 10 158–10 163, Sep. 2003.

[8] K. Golman, J. H. Ardenkjær-Larsen, J. S. Petersson, S. Mansson, and I. Leunbach, "Molecular imaging with endogenous substances," *Proceedings of the National Academy of Sciences*, vol. 100, no. 18, pp. 10 435–10 439, 2003.

[9] Y. Xing, G. D. Reed, J. M. Pauly, A. B. Kerr, and P. E. Larson, "Optimal variable flip angle schemes for dynamic acquisition of exchanging hyperpolarized substrates," *Journal of Magnetic Resonance*, vol. 234, pp. 75–81, 2013.

[10] S. I. Machingal, "Sampling strategies for hyperpolarized carbon-13 imaging," Master's thesis, University of California, San Francisco, USA, 2014.

[11] R. F. Schulte, J. I. Sperl, E. Weidl, M. I. Menzel, M. A. Janich, O. Khegai, M. Durst, J. H. Ardenkjaer-Larsen, S. J. Glaser, A. Haase, M. Schwaiger, and F. Wiesinger, "Saturation-recovery metabolic-exchange rate imaging with hyperpolarized [1-^{13}C] pyruvate using spectral-spatial excitation," *Magnetic Resonance in Medicine*, vol. 69, no. 5, pp. 1209–1216, 2013.

[12] J. Lygeros, C. Tomlin, and S. Sastry, "Hybrid systems: Modeling, analysis and control," UC Berkeley / ETH Zurich lecture notes, 2008. [Online]. Available: https://web.archive.org/web/20100723205138/http://www-inst.cs.berkeley.edu/~ee291e/sp09/handouts/book.pdf

[13] R. Goebel, R. Sanfelice, and A. R. Teel, *Hybrid Dynamical Systems: Modeling, Stability, and Robustness*. Princeton University Press, 2012.

[14] C.-T. Chen, *Linear System Theory and Design*, 3rd ed. New York, NY, USA: Oxford University Press, Inc., 1998.

[15] H. Gudbjartsson and S. Patz, "The Rician distribution of noisy MRI data," *Magnetic Resonance in Medicine*, vol. 34, no. 6, pp. 910–914, 1995.

[16] F. Pukelsheim, *Optimal design of experiments*, ser. Probability and mathematical statistics. Wiley, 1993.

[17] H. Cramér, *Mathematical Methods of Statistics*. Princeton University Press, 1946.

[18] J. Maidens, P. Larson, and M. Arcak, "Optimal experiment design for physiological parameter estimation using hyperpolarized carbon-13 magnetic resonance imaging," in *Proceedings of the American Control Conference*, 2015.

[19] M. J. Albers, R. Bok, A. P. Chen, C. H. Cunningham, M. L. Zierhut, V. Y. Zhang, S. J. Kohler, J. Tropp, R. E. Hurd, Y.-F. Yen, S. J. Nelson, D. B. Vigneron, and J. Kurhanewicz, "Hyperpolarized ^{13}C lactate, pyruvate, and alanine: Noninvasive biomarkers for prostate cancer detection and grading," *Cancer Research*, vol. 68, no. 20, pp. 8607–8615, 2008.

[20] M. A. Schroeder, L. E. Cochlin, L. C. Heather, K. Clarke, G. K. Radda, and D. J. Tyler, "In vivo assessment of pyruvate dehydrogenase flux in the heart using hyperpolarized carbon-13 magnetic resonance," *Proceedings of the National Academy of Sciences*, vol. 105, no. 33, pp. 12 051–12 056, 2008.

[21] É. Walter and L. Pronzato, *Identification of parametric models from experimental data*, ser. Communications and control engineering. Springer, 1997.

[22] The MathWorks, Inc., "MATLAB and Optimization Toolbox Release 2013b," Natick, Massachusetts, United States.

[23] J. Nocedal and S. Wright, *Numerical Optimization*. Springer, 2006.

[24] J. W. Gordon, S. Machingal, J. Kurhanewicz, D. Vigneron, and P. Larson, "Ramp-sampled, symmetric EPI for rapid dynamic metabolic imaging of hyperpolarized ^{13}C substrates on a clinical MRI scanner," in *Proceedings of the 23rd Annual Meeting of ISMRM, Toronto, Ontario, Abstract 4717*, 2015.

[25] L. Zhao, R. Mulkern, C.-H. Tseng, D. Williamson, S. Patz, R. Kraft, R. L. Walsworth, F. A. Jolesz, and M. S. Albert, "Gradient-echo imaging considerations for hyperpolarized ^{129}Xe MR," *Journal of Magnetic Resonance, Series B*, vol. 113, no. 2, pp. 179 –183, 1996.

[26] D. W. McRobbie, R. A. Lerski, and K. Straughan, "Slice profile effects and their calibration and correction in quantitative NMR imaging," *Physics in Medicine and Biology*, vol. 32, no. 8, pp. 971 – 983, 1987.

[27] M. H. Deppe, K. Teh, J. Parra-Robles, K. J. Lee, and J. M. Wild, "Slice profile effects in 2D slice-selective MRI of hyperpolarized nuclei," *Journal of Magnetic Resonance*, vol. 202, no. 2, pp. 180 – 189, 2010.